2022 IEEE Conference on Control Technology and Applications (CCTA)
August 22-25, 2022. Trieste, Italy

Robust Nonlinear Control of Fluid Flow Fields Using a Barrier function-based Sliding Mode Control Approach

Anu Kossery Jayaprakash [1,*] and William MacKunis [2]

***Abstract*— A barrier function-based sliding mode control method is developed for fluid flow dynamic systems, which formally compensates for the model parameter variations resulting from actuator perturbations that are inherent in closed-loop active flow control applications. In an effort to reduce chattering, the control law incorporates adaptive sliding gain terms based on barrier functions. To the best of the authors' knowledge, this is the first barrier function-based nonlinear closed-loop active flow control result to prove finite-time real sliding of a reduced-order flow dynamic system, which formally incorporates input-multiplicative time-varying parametric uncertainty. An innovative error system development is provided along with a rigorous Lyapunov-based stability analysis to prove the theoretical results. A detailed comparative numerical study is also provided, which shows the significant reduction in mean squared error that are achieved using the barrier function-based control law over a standard sliding mode controller.**

I. INTRODUCTION

Considerable challenges exist in designing controllers for fluid flow systems due to the fact that the governing dynamic equations (i.e., the Navier-Stokes equations) are in a form that is not control-amenable. To address this issue, various techniques can be utilized to obtain reduced-order models of the fluid flow dynamics. A key challenge in control design based on reduced-order models (ROMs) of fluid flow dynamic systems is that the resulting models are in a highly non-standard mathematical form containing unmodeled parameter fluctuations, actuator model uncertainty, and nonlinear coupling between the state and control input. While numerous methods have been presented to achieve control of fluid flow, there remain several open problems to be addressed in closed-loop nonlinear control of fluid dynamic systems. Specifically, there remains a need for closed-loop flow control methods that formally incorporate the complete actuation dynamics and actuator perturbations in the ROM.

A. Motivation

The two most broad categories of flow control configurations can be classified as **passive flow control (PFC)** [1], [2] or **active flow control (AFC)**. Active control can be further categorized as open-loop In order to achieve reliable performance over a wide range of operating conditions, closed-loop AFC offers many potential benefits over PFC and open loop AFC methods.

[1]Anu Kossery Jayaprakash*, Ph.D candidate, Physical Sciences Department, Embry Riddle Aeronautical University, Daytona Beach, FL 32114. kosserya@my.erau.edu

[2]William MacKunis, Associate Professor, Physical Sciences Department, Embry Riddle Aeronautical University, Daytona Beach, FL 32114. mackuniw@erau.edu

B. Literature Survey

Sliding mode control methods are popularly utilized to achieve improved robustness in closed-loop control systems. However, practical implementation of discontinuous sliding mode control methods is significantly hindered by the well-known chattering phenomenon. As an alternative, barrier function-based control techniques have been recently investigated in [3], [4], [5]. In [3] a class K_∞ function-based adaptive sliding mode control scheme is presented, which is shown to reduce the chattering and overestimation phenomena that commonly occur in classical adaptive sliding mode control. The results in [3] describe the closed-loop performance using both concave and convex barrier functions. Barrier function-based control laws specifically designed for safety critical systems are presented in [4] and [5]. The aforementioned recent results have clearly demonstrated that barrier function-based adaptive sliding mode control can achieve significant performance improvements over standard sliding mode control for a variety of applications. Based on this, the current result investigates the performance improvement that can be achieved by using a barrier function-based fluid flow control method for an uncertain nonlinear parameter-varying POD-based ROM, which formally incorporates input-multiplicative parametric uncertainty and actuator perturbations.

Sliding mode estimation and flow control methods were presented in our recent work [6], [7], [8]. The current result presents a non-trivial extension of our previous results, in which we develop a barrier function-based sliding mode control method that is based on a detailed POD-based ROM of the complete actuated flow field dynamics. To achieve the result, a non-trivial reworking of the error system development, control design, and rigorous stability analysis are presented along with a detailed numerical study.

C. Contribution

In this paper, a barrier function-based sliding mode control design is presented, which is rigorously proven to achieve finite-time real sliding in a fluid flow dynamic system. To the best of the authors' knowledge, this is the first barrier function-based nonlinear closed-loop AFC result to prove finite-time real sliding of a POD-based reduced-order model for the complete actuated flow field dynamics, which formally incorporates both input-multiplicative time-varying parametric uncertainty and nonlinear couplings between the state and control input. A rigorous Lyapunov-based stability analysis is utilized to prove the theoretical result. A comparative numerical study is also provided to demonstrate the

2022 IEEE Conference on Control Technology and Applications (CCTA) | 978-1-6654-7338-5/22/$31.00 ©2022 IEEE | DOI: 10.1109/CCTA49430.2022.9966013

performance of the proposed barrier function-based control method over a standard sliding mode control law.

II. Dynamic Model and Properties

In this section, a POD-based model reduction technique is summarized to derive the ROM that will be utilized in the control design.

A. Reduced order Model for Flow Field Dynamics

The incompressible Navier-Stokes equations are given as [9]

$$\nabla \cdot u = 0, \qquad \frac{\partial u}{\partial t} = -(u \cdot \nabla)u + \frac{1}{Re}\nabla^2(u) - \nabla p \quad (1)$$

where $u(s,t) : \Gamma \times [0,\infty) \in \mathbb{R}^3$ denotes the velocity of the flow field over a spatial domain $s \in \Gamma \subset \mathbb{R}^3$; $p(s,t) \in \mathbb{R}^3$ is the space- and time-dependent pressure of the flow field over Γ ; and Re denotes the Reynolds number.

In the POD technique, the flow velocity field $u(s,t)$ is expanded as a weighted sum of actuated and unactuated POD modes defined over a spatial domain Γ. The actuation effects are embedded in the coefficients of the Galerkin system. Specifically, the actuation effects can be included in the reduced-order model by defining the modal decomposition as [7]

$$u(s,t) = u_0 + \sum_{i=1}^{n} x_i(t)\phi_i(s) + \sum_{i=1}^{m} \gamma_i(t)\psi_i(s) \quad (2)$$

In (2), $\phi_i(s) \in \mathbb{R}^3$, $i = 1,...,n$, denote the unactuated POD modes and $x_i(t)$, $i = 1,...,n$, denote time-varying coefficients resulting from the modal decomposition; and $u_0 \in \mathbb{R}^3$ denotes the mean flow velocity over Γ; $\psi_i(s) \in \mathbb{R}$ denote the actuation modes, and $\gamma_i(t) \in \mathbb{R}$ denote actuation values (i.e., control inputs). By leveraging an input separation method similar to that in [10], [11], the actuation modes can be defined as the modes that minimize the energy not captured in the modal expansion of the actuated flow field.

By substituting the decomposition in (2) into (1), the complete actuated POD-based reduced-order model is obtained as

$$\begin{aligned} \dot{x}_k &= A_k + \sum_{i=1}^{n} B_{ki}x_i(t) + \sum_{i=1}^{n}\sum_{j=1}^{n} C_{kij}x_i(t)x_j(t) \\ &\quad + \sum_{i=1}^{m} D_{ki}\dot{\gamma}_i(t) + \sum_{i=1}^{n}\sum_{j=1}^{m} E_{kij}x_i(t)\gamma_j(t) \\ &\quad + \sum_{i=1}^{m} F_{ki}\gamma_i(t) + \sum_{i=1}^{m}\sum_{j=1}^{m} G_{kij}\gamma_i(t)\gamma_j(t) \end{aligned} \quad (3)$$

In (3), $A_k(t)$, $B_{ki}(t)$, $C_{kij}(t) \in \mathbb{R}$, for $k,i,j = 1,...,n$; $D_{ki}(t)$, $F_{ki}(t)$, $G_{kij}(t)$, $k,i,j = 1,...,m$; and $E_{kij}(t) \in \mathbb{R}$, for $k,i = 1,...,n$, and for $j = 1,...\ m$, represent time-varying uncertain parameters, the nominal values of which can be explicitly computed for any given, fixed set of numerical or experimental flow field data. Also in (3), $\dot{\gamma}_i(t)$, $i = 1,...,n$, represent the elements of the control input vector, which can be physically interpreted as a controllable perturbation to the flow field.

Remark 1. ***(Inherent Parameter Variations)*** *The POD-based ROM in (3) formally incorporates actuator perturbations through the time variation in the parameters $A(t),...,G(t)$. Compensation for the time-varying parametric uncertainty in the ROM is of crucial importance for reliable closed-loop flow control design.*

Remark 2. ***(Unmeasurable State)*** *The model coefficients $x_i(t)$, for $i = 1,...,n$, in the reduced-order model (3) are unmeasurable in actual implementation. Estimator design is not the focus of the current work, so it will be assumed here that state estimates are available for feedback. Readers are referred to [6], [7], [12] for details on relevant estimator design methods.*

B. Control-oriented Flow Dynamic Model

To facilitate the subsequent control design procedure and analysis, the ROM in (3) will be rewritten in control-oriented form as

$$\begin{aligned} \dot{x} &= f_1(x,x,\theta_1(t)) + f_2(x,\gamma,\theta_2(t)) \\ &\quad + f_3(\gamma,\gamma,\theta_3(t)) + \Omega(t)v \end{aligned} \quad (4)$$

where $f_1(\cdot)$, $f_2(\cdot)$, $f_3(\cdot) \in \mathbb{R}^n$ denote uncertain nonlinear (quadratic) terms for which the k^{th} rows are explicitly defined as

$$f_{1,k}(x,\theta_1(t)) \triangleq A_k + \sum_{i=1}^{n} B_{ki}x_i(t) + \sum_{i=1}^{n}\sum_{j=1}^{n} C_{kij}x_i(t)x_j(t) \quad (5)$$

$$f_{2,k}(x,\gamma,\theta_2(t)) \triangleq \sum_{i=1}^{n}\sum_{j=1}^{m} E_{kij}x_i(t)\gamma_j(t) \quad (6)$$

$$f_{3,k}(\gamma,\theta_3(t)) \triangleq \sum_{i=1}^{m} F_{ki}\gamma_i(t) + \sum_{i=1}^{m}\sum_{j=1}^{m} G_{kij}\gamma_i(t)\gamma_j(t) \quad (7)$$

for $k = 1,...,n$. In (4), $x(t) \triangleq [\ x_1(t) \quad \cdots \quad x_n(t)\ ]^T \in \mathbb{R}^n$ denotes the state vector, $v(t) \triangleq \dot{\gamma}(t) \in \mathbb{R}^m$ is the control input; and $\theta_1(t) \in \mathbb{R}^{n^2+n+1}$, $\theta_2(t) \in \mathbb{R}^{n^2}$, $\theta_3(t) \in \mathbb{R}^{n^2+n}$, for $k = 1,...,n$, denote vectors containing the uncertain time-varying parameters in the dynamic model. Also in (4), $\Omega(t) \in \mathbb{R}^{n\times m}$ denotes an uncertain input gain matrix. Specifically, $\Omega(t)$ contains the terms D_{ki}, for $k = 1,...,n$, $i = 1,...,m$, which are introduced in (3).

Assumption 1. *The reduced-order model in (4) is assumed to be controllable.*

Assumption 2. *The parameter vectors $\theta_1(t)$, $\theta_2(t)$, $\theta_3(t)$ and the parameter matrix $\Omega(t)$ and their derivatives satisfy the following inequalities:*

$$\begin{aligned} &\|\theta_1(t)\| \le \zeta_1 \quad \|\theta_2(t)\| \le \zeta_2 \quad \|\theta_3(t)\| \le \zeta_3 \\ &\|\dot{\theta}_1(t)\| \le \zeta_{1d} \quad \|\dot{\theta}_2(t)\| \le \zeta_{2d} \quad \|\dot{\theta}_3(t)\| \le \zeta_{3d} \\ &\sup_t\{\|\Omega(t)\|_{i\infty}\} \le \zeta_\Omega \quad \sup_t\{\|\dot{\Omega}(t)\|_{i\infty}\} \le \zeta_{\Omega d} \end{aligned} \quad (8)$$

where ζ_1, ζ_2, ζ_3, ζ_Ω, ζ_{1d}, ζ_{2d}, ζ_{3d}, $\zeta_{\Omega d} \in \mathbb{R}^+$ are known bounding constants. In the subsequent stability analysis, we will utilize the known bounds on the parameters to derive sufficient gain conditions to achieve the desired control objective.

Assumption 3. ***(Fully Actuated System)*** *The control design and stability analysis presented here are applicable to any system for which $m \geq n$, but it will be assumed that $m = n$ without loss of generality.*

III. Control Development

A. Control Objective

The control objective is to ensure that the state $x(t)$ tracks a desired flow field velocity profile $x_d(t) \in \mathbb{R}^n$. To quantify this control objective, a tracking error variable $e(t) \in \mathbb{R}^n$ is defined as

$$e \triangleq x - x_d. \tag{9}$$

To facilitate the subsequent analysis, an auxiliary (filtered) tracking error variable, denoted by $r(t) \in \mathbb{R}^n$, is defined as

$$r \triangleq \dot{e} + \alpha e \tag{10}$$

where $\alpha \in \mathbb{R}$ is a positive, constant control gain. (Note that α could also be defined as a control gain matrix.)

Assumption 4. *The desired flow field velocity profile $x_d(t)$ is bounded and smooth in the sense that*

$$x_d(t) \leq \zeta_{xd1}, \qquad \dot{x}_d(t) \leq \zeta_{xd2}, \qquad \ddot{x}_d(t) \leq \zeta_{xd3} \tag{11}$$

where $\zeta_{xd1},\ \zeta_{xd2},\ \zeta_{xd3} \in \mathbb{R}^+$ are known bounding constants.

Lemma 1. *If $|r(t_1)| \leq \sigma_{cv}$, at some finite time instant $t_1 > 0$, where $\sigma_{cv} \in \mathbb{R}^+$ is a bounding constant, then Equation (10) can be used to prove that the tracking error $e(t)$ is bounded as*

$$\exp(-\alpha t_1)|e(0)| - \frac{\sigma_{cv}}{\alpha} < |e(t)| < \exp(-\alpha t_1)|e(0)| + \frac{\sigma_{cv}}{\alpha} \tag{12}$$

for $t \geq t_1$, where α is a control gain defined as in (10). Hence, the ultimate bound on the tracking error $e(t)$ can be made arbitrarily small by adjusting α.

Proof: By using Equation (10), the following can be obtained:

$$|r(t)| \leq \sigma_{cv} \Rightarrow |\dot{e}(t) + \alpha e(t)| \leq \sigma_{cv} \tag{13}$$

By eliminating the absolute value operation and rearranging, Inequality (13) can be expressed as

$$\dot{e}(t) \leq -\alpha e(t) + \sigma_{cv}, \qquad \dot{e}(t) \geq -\alpha e(t) - \sigma_{cv}. \tag{14}$$

The solution to the linear differential inequalities in (14) is straightforward and can be obtained as

$$e(t) \leq e(0)\exp(-\alpha t) + \frac{\sigma_{cv}}{\alpha}(1 - \exp(-\alpha t)) \tag{15}$$

$$e(t) \geq e(0)\exp(-\alpha t) - \frac{\sigma_{cv}}{\alpha}(1 - \exp(-\alpha t)) \tag{16}$$

Thus, by using the fact that $1 - \exp(-\alpha t) \leq 1$, one obtains

$$\exp(-\alpha t)|e(0)| - \frac{\sigma_{cv}}{\alpha} < |e(t)| < \exp(-\alpha t)|e(0)| + \frac{\sigma_{cv}}{\alpha} \tag{17}$$

Inequalities (12) can be directly inferred from (17) for any $t > t_1 > 0$.

Lemma (1) will be utilized in the subsequent stability analysis.

B. Open-Loop Error System

The open-loop tracking error dynamics can be developed by taking the time derivative of (10) and using (4)–(9) to obtain

$$\dot{r} = \tilde{N} + \tilde{N}_\gamma + N_d + \dot{\Omega} v + \Omega \dot{v} \tag{18}$$

where the uncertain nonlinear auxiliary terms $\tilde{N}(x, \dot{x}, x_d, \dot{x}_d, e, r, t) \in \mathbb{R}^n$, $\tilde{N}_\gamma(x, \dot{x}, \gamma) \in \mathbb{R}^n$, and $N_d(x_d, \dot{x}_d, \ddot{x}_d)$ are explicitly defined as

$$\tilde{N}_\gamma \triangleq \gamma^T E_k^T \dot{x} + x^T \dot{E}_k \gamma + \dot{F}_k \gamma + \gamma^T \dot{G}_k \gamma \tag{19}$$

$$\begin{aligned} \tilde{N} \triangleq\ & \dot{B}_k(x - x_d) + B_k(\dot{x} - \dot{x}_d) + x^T(C_k + C_k^T)\dot{x}_d \\ & -x_d^T(C_k + C_k^T)\dot{x}_d + x^T(C_k + C_k^T)\dot{x} \\ & -x^T(C_k + C_k^T)\dot{x}_d + x^T\dot{C}_k x - x_d^T\dot{C}_k x_d + \alpha(r - \alpha e) \end{aligned} \tag{20}$$

$$\begin{aligned} N_d =\ & \dot{B}_k x_d + B_k \dot{x}_d + x_d^T(C_k + C_k^T)\dot{x}_d \\ & + x_d^T \dot{C}_k x_d - \ddot{x}_d \end{aligned} \tag{21}$$

Motivation for the selective grouping of terms in (19)–(21) is based on the fact that the following bounding inequalities can be developed:

$$\|\tilde{N}\| \leq \eta_{z1}\|z\| + \eta_{z2}\|z\|^2 \tag{22}$$

$$\|N_d\| \leq \zeta_{Nd} \tag{23}$$

$$\|\tilde{N}_\gamma\| \leq \Xi_1\|\gamma\|^2 + \Xi_2\|\gamma\| + \Xi_3\|z\| + \Xi_4\|z\|^2 \tag{24}$$

where $\eta_{z1}, \eta_{z2}, \zeta_{Nd},\ \Xi_1,\ \Xi_2,\ \Xi_3,\ \Xi_4 \in \mathbb{R}^+$ are known bounding constants; and $z(t) \in \mathbb{R}^{2n}$ is defined as

$$z \triangleq \begin{bmatrix} e^T & r^T \end{bmatrix}^T. \tag{25}$$

Note that the bounding of $N_d(x_d, \dot{x}_d, \ddot{x}_d)$ follows directly from Assumption 4 and Inequalities (11).

C. Control Design and Closed-loop Error System

To facilitate the subsequent control development and stability analysis, definitions of the herein-employed barrier function will first be presented. For detailed mathematical definitions of barrier functions, readers are referred to [13].

1) Convex Barrier Function [3]: The convex barrier function being considered in the current result can be expressed as

$$k_{bf,i}(|\xi|) = \rho_i \left(\exp\left(\frac{|\xi|}{\lambda_i} \right) - 1 \right), \qquad i = 1, ..., 6 \tag{26}$$

for all $\xi \in \mathbb{R}^n$, where ρ_i and λ_i are positive parameters. $k_{bf,i}(\cdot)$ is a strictly increasing convex function on $(0, +\infty)$, since $k'_{bf,i}(|\xi|) = \frac{\rho_i}{\lambda_i}\exp(\frac{|\xi|}{\lambda_i})$ and the second order derivative $k''_{bf,i}(|\xi|) = \frac{\rho_i}{\lambda_i^2}\exp(\frac{|\xi|}{\lambda_i})$ on $[0, \infty)$ for $i = 1, ..., 6$.

Lemma 2. *Control gains can be selected to ensure that the convex barrier function defined in (26) satisfies the inequalities*

$$k_{bf,i}(|\xi|) \geq c_1\|\xi\|, \quad \forall \xi \in \mathbb{R}^n \tag{27}$$

$$k_{bf,i}(|\xi|) \geq c_2\|\xi\|^2, \quad \forall \xi \in \mathbb{R}^n \tag{28}$$

where $c_1, c_2 \in \mathbb{R}^+$ are known bounding constants.

Proof: It is sufficient to prove that the following conditions for a convex barrier function $k_{bf,i}(|\xi|)$, $\forall \xi \in \mathbb{R}^n$, are satisfied, where $k_{bf,i}(\cdot)$ is defined as in (26):

***Condition 1**:*

$$\lim_{\xi \to 0^+} \frac{\partial}{\partial \xi} k_{bf,i}(|\xi|) > \lim_{\xi \to 0^+} \frac{\partial}{\partial \xi}(c_i\|\xi\|^j) \tag{29}$$

***Condition 2**:*

$$\lim_{\xi \to 0^+} \frac{\partial^2}{\partial \xi^2} k_{bf,i}(|\xi|) > \lim_{\xi \to 0^+} \frac{\partial^2}{\partial \xi^2}(c_i\|\xi\|^j) \tag{30}$$

where $i, j = 1, 2$.

***Condition 3**: The function $k_{bf,i}(|\xi|)$ is a strictly increasing convex barrier function.*

Conditions 1 and 2 can be proved by calculating the first and second derivatives of $k_{bf,i}(|\xi|)$ in (26) as follows: For the $j = 1$ case in (27), one obtains (Condition 1) $\frac{\rho_i}{\lambda_i} > c_1$ and (Condition 2) $\frac{\rho_i}{\lambda_i^2} > 0$; and for the $j = 2$ case in (28), one obtains (Condition 1) $\frac{\rho_i}{\lambda_i} > 0$ and (Condition 2) $\frac{\rho_i}{\lambda_i^2} > 2c_2$. Clearly, control gains ρ_i and λ_i can be selected to satisfy these inequalities; thus Conditions 1 and 2 are satisfied. The symmetry of $k_{bf,i}(\cdot)$ (i.e., $k_{bf,i}(\cdot)$ is an even function) can be leveraged to prove the claims in (27) and (28). Condition 3 holds by definition.

Based on the open loop error dynamics in (18) and the subsequent stability analysis, the control input is designed via the implicit learning law

$$\begin{aligned} \dot{v} &= -\Omega_0^{-1}\Big(K_{bf,1}(|r|) + K_{bf,2}(|v|) + K_{bf,3}(|\gamma|) \\ &\quad + K_{bf,4}(|\gamma|) + K_{bf,5}(|z|) + K_{bf,6}(|z|)\Big)\,\mathrm{sgn}(r) \end{aligned} \tag{31}$$

where $K_{bf,i}(\cdot)$, $i = 1, ..., 6$, denote diagonal matrices containing barrier functions $k_{bf,i}(\cdot)$ as described in (26).

In (32), $\Omega_0 \in \mathbb{R}^{n\times n}$ is a matrix containing the constant, known, nominal values of the uncertain parameters in Ω; and $\mathrm{sgn}(\cdot)$ denotes the standard signum function, where the function is applied element-wise to the vector argument.

After substituting (32) into the open-loop error dynamics in (18), the closed-loop error system can be expressed as

$$\begin{aligned} \dot{r} &= \tilde{N} + \tilde{N}_\gamma + N_d + \dot{\Omega}v - \tilde{\Omega}(K_{bf,1}(|r|) + K_{bf,2}(|v|) \\ &\quad + K_{bf,3}(|\gamma|) + K_{bf,4}(|\gamma|) + K_{bf,5}(|z|) \\ &\quad + K_{bf,6}(|z|))\,\mathrm{sgn}(r) \end{aligned} \tag{32}$$

In (32), the uncertain parameter mismatch matrix $\tilde{\Omega}(t) \in \mathbb{R}^{n\times n}$ is defined as

$$\tilde{\Omega} \triangleq \Omega\Omega_0^{-1}. \tag{33}$$

To facilitate the subsequent stability analysis, the mismatch matrix $\tilde{\Omega}(t)$ in (33) will be separated into diagonal ($\Lambda(t) \in \mathbb{R}^{n\times n}$) and off-diagonal ($\Delta(t) \in \mathbb{R}^{n\times n}$) components as

$$\tilde{\Omega} = \Lambda + \Delta. \tag{34}$$

Assumption 5. *Approximate knowledge of the parameter matrix $\Omega(t)$ is available such that the mismatch matrix $\tilde{\Omega}(t)$ is diagonally dominant in the sense that*

$$\inf_t\{\lambda_{\min}(\Lambda)\} - \sup_t\{\|\Delta\|_{i\infty}\} > \varepsilon \tag{35}$$

where $\varepsilon \in \mathbb{R}^+$ is a known bounding constant.

Assumption 5 is mild in the sense that, for a given set of flow field data (e.g., from high-fidelity CFD simulation or experiment), the nominal values of the reduced-order model parameters would be readily available.

IV. Stability Analysis

Theorem 1. *The control law given in Equation (32) ensures convergence to the real sliding surface $|r(t)| \leq \sigma_{cv}$ in finite time, where σ_{cv} can be made arbitrarily small, provided the barrier function matrices $K_{bf,i}$, for $i = 1, ..., 6$, are designed to satisfy the sufficient conditions*

$$\lambda_{\min}(K_{bf,1}) > \frac{\zeta_{Nd}}{\varepsilon} \qquad \lambda_{\min}(K_{bf,2}) > \frac{\zeta_{\Omega d}}{\varepsilon}\|v\| \tag{36}$$

$$\lambda_{\min}(K_{bf,3}) > \frac{\Xi_1}{\varepsilon} \qquad \lambda_{\min}(K_{bf,4}) > \frac{\Xi_2}{\varepsilon} \tag{37}$$

$$\lambda_{\min}(K_{bf,5}) > \frac{\eta_{z_1} + \Xi_3}{\varepsilon} \qquad \lambda_{\min}(K_{bf,6}) > \frac{\eta_{z_2} + \Xi_4}{\varepsilon} \tag{38}$$

where $\zeta_{\Omega d}$, ζ_{Nd}, Ξ_1, Ξ_2, Ξ_3, Ξ_4, η_{z1} and η_{z2} are introduced in (22) – (24); ε is introduced in (35); and $\lambda_{\min}(\cdot)$ denotes the minimum eigenvalue of the argument.

Proof: Let $V(r) : \mathbb{R}^n \to \mathbb{R}$ be a continuously differentiable, positive-definite function defined as

$$V(r) \triangleq \frac{1}{2} r^T r \tag{39}$$

By utilizing bounding inequalities (8) and (35) of Assumptions 2 and 5, the following inequalities can be developed.

$$\begin{aligned} -r^T\Big(\Lambda + \Delta\Big)K_{bf,1}(|r|)\,\mathrm{sgn}(r) &\leq -\varepsilon\lambda_{\min}(K_{bf,1})|r| \\ -r^T\Big(\Lambda + \Delta\Big)K_{bf,2}(|v|)\,\mathrm{sgn}(r) &\leq -\varepsilon\lambda_{\min}(K_{bf,2})|r| \\ -r^T\Big(\Lambda + \Delta\Big)K_{bf,3}(|\gamma|)\,\mathrm{sgn}(r) &\leq -\varepsilon\lambda_{\min}(K_{bf,3})|r| \\ -r^T\Big(\Lambda + \Delta\Big)K_{bf,4}(|\gamma|)\,\mathrm{sgn}(r) &\leq -\varepsilon\lambda_{\min}(K_{bf,4})|r| \\ -r^T\Big(\Lambda + \Delta\Big)K_{bf,5}(|z|)\,\mathrm{sgn}(r) &\leq -\varepsilon\lambda_{\min}(K_{bf,5})|r| \\ -r^T\Big(\Lambda + \Delta\Big)K_{bf,6}(|z|)\,\mathrm{sgn}(r) &\leq -\varepsilon\lambda_{\min}(K_{bf,6})|r| \end{aligned} \tag{40}$$

After taking the time derivative of (39) and using Equations (32), (33), (22), (23), (24), (40), and by using Lemma

1 and the sufficient gain conditions for $K_{bf,i}$, for $i = 1, ..., 6$ in (36) - (38), the upper bound of $\dot{V}(r)$ can be expressed as

$$\dot{V}(r) \leq -\left[\varepsilon\lambda_{\min}(K_{bf,1}(|r|)) - \zeta_{Nd}\right]\|r\| \tag{41}$$

where the fact that $|r| \geq \|r\| \ \forall \ r \in \mathbb{R}^n$ was used. The upper bound can be expressed in a more compact form as

$$\dot{V}(r) \leq -\beta_{cv}\|r\|, \ \beta_{cv} \triangleq \varepsilon_1 K_{bf,\min}(|r|) - \zeta_{Nd} \tag{42}$$

where $K_{bf,\min}(|r|) \triangleq \lambda_{\min}(K_{bf,1}(|r|))$. Thus, Inequality (42) can be used to prove finite-time convergence to the real sliding surface $|r| \leq \sigma_{cv}$. Specifically, the barrier function definition in (26) can be used to explicitly calculate the ultimate bound σ_{cv} by using (42) to obtain the following condition for convergence:

$$\varepsilon K_{bf,\min}(|r|) - \zeta_{Nd} > 0. \tag{43}$$

By using the convex barrier function definition in (26), the inequality can be expressed as

$$\varepsilon\rho_1\left(\exp\left(\frac{|r|}{\lambda_1}\right) - 1\right) > \zeta_{Nd}$$

Thus, the region of convergence σ_{cv} can be explicitly calculated as

$$\exp\left(\frac{|r|}{\lambda_1}\right) - 1 > \frac{\zeta_{Nd}}{\varepsilon\rho_1} \tag{44}$$

$$\Rightarrow \frac{|r|}{\lambda_1} > \ln\left(\frac{\zeta_{Nd}}{\varepsilon\rho_1} + 1\right) \tag{45}$$

$$\Rightarrow |r| > \lambda_1\left(\ln\left(\frac{\zeta_{Nd}}{\varepsilon\rho_1} + 1\right)\right) \tag{46}$$

$$|r| \leq \sigma_{cv} \tag{47}$$

$$\sigma_{cv} = \lambda_1\left(\ln\left(\frac{\zeta_{Nd}}{\varepsilon\rho_1} + 1\right)\right) \tag{48}$$

Hence, (48) can be used to prove that the region of convergence can be made arbitrarily small by adjusting the control gains λ_1 and ρ_1. By using Lemma 1, it further follows from (48) that the tracking error $e(t)$ converges in finite time to the bounded set described by (17).

V. Simulation

A detailed numerical simulation was created using Matlab/ Simulink to demonstrate the performance of the proposed robust control law. The simulation demonstrates the performance of the control law in (32) for two cases: 1) with barrier function and 2) without barrier function. The flow field dynamic reduced-order model used in this simulation is given by [14]:

$$\begin{aligned}
\dot{x_1} &= b_1(t) + L_{11}(t)x_1 + Q_{141}(t)x_1x_4 + Q_{111}(t)x_1^2 \\
&\quad + Q_{121}(t)x_1x_2 + Q_{131}(t)x_1x_3 + \beta_1(t)\dot{\gamma_1} \qquad (49)\\
\dot{x_2} &= b_2(t) + [L_{22}(t) + R_2(t)(x_2^2 + x_3^2)]x_2 + L_{23}(t)x_3 \\
&\quad + Q_{212}(t)x_1x_2 + \beta_2(t)\dot{\gamma_2} \qquad (50)\\
\dot{x_3} &= b_3(t) + L_{32}(t)x_2 + [L_{33}(t) + R_3(x_2(t)^2 + x_3^2)]x_3 \\
&\quad + Q_{313}(t)x_1x_3 + Q_{314}(t)x_1x_4 + \beta_3(t)\dot{\gamma_3} \qquad (51)\\
\dot{x_4} &= b_4(t) + L_{41}(t)x_1 + L_{44}(t)x_4 + Q_{444}(t)x_4^2 \\
&\quad + Q_{414}(t)x_1x_4(t) + Q_{424}(t)x_2x_4 \\
&\quad + Q_{434}(t)x_3x_4 + \beta_4(t)\dot{\gamma_4} \qquad (52)
\end{aligned}$$

To simulate a realistic closed-loop AFC scenario where the model parameters are influenced by the control perturbations, the parameters in the plant model in (49)–(52) are time-varying. For completeness in defining the simulation plant model, the initial values of the time varying parameters $b_i(t), L_{ij}(t), Q_{ijk}(t)$ for $i, j, k = 1, ..., 4$ are provided in Table I and were taken from [14]. The initial conditions of the states are $x_{10} = 2, x_{20} = 3, x_{30} = 6, x_{40} = 2$.

A. Summary of Results

The numerical simulation is based on concave barrier functions defined as $k_{bf,i} = \rho_i \ln(\frac{|r|}{\lambda_i} - 1))$. Note that the use of concave barrier functions as opposed to convex is valid, since Lemma 2 in the previous proof provides *sufficient* not *necessary* conditions for the barrier functions used in the control design. The control gains in the simulation were selected as $\alpha = 50, \rho_r = 500 \times I_4, \lambda_r = 1, \rho_v = 10 \times I_4, \lambda_v = 1, \rho_{\gamma 1} = 1000 \times I_4, \lambda_{\gamma 1} = 3, \rho_{\gamma 2} = 10 \times I_4, \lambda_{\gamma 2} = 1, \rho_{z1} = 0.01 \times I_4; \lambda_{z1} = 100, \rho_{z2} = 0.001 \times I_4, \lambda_{z2} = 100.$

Figure 1 shows the comparison of the time evolution of the states during closed-loop operation for proposed controller with and without barrier function under 20% uncertainty, and Figure 2 shows the corresponding control input. This plot clearly shows the benefit of using barrier function over constant gains in the control law. Figure 3 shows a bar graph of the average MSE over the 10 iterations for each of six levels of parametric uncertainty.

VI. Conclusion

A barrier function-based sliding mode control method is applied to a detailed ROM of the complete actuated dynamics of a fluid flow dynamic system in the presence of parametric uncertainty in the plant model and the actuation model. A rigorous Lyapunov-based stability analysis is utilized to prove that the proposed barrier function-based control law achieves finite-time real sliding in the presence of time-varying input-multiplicative parametric uncertainty and nonlinear coupling between the state and control input.

To further demonstrate the performance of the barrier function-based robust nonlinear control law, a detailed comparative numerical study is provided, which shows the performance of the proposed barrier function-based sliding mode

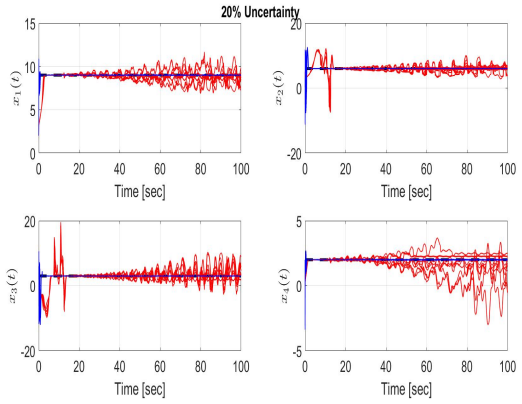

Fig. 1. Time evolution of the state $x_1(t), x_2(t), x_3(t), x_4(t)$ for controller without barrier function (**red**) and controller with barrier function (**blue**) during closed-loop operation for 10 iterations of randomized uncertainty.

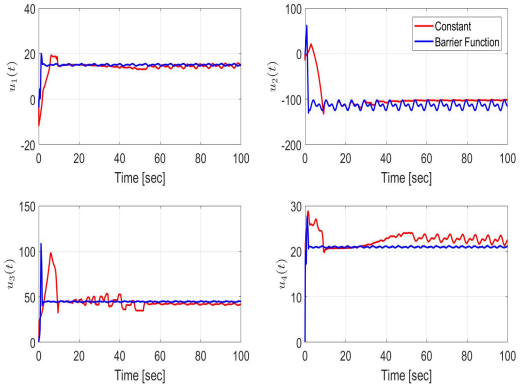

Fig. 2. Closed loop response of the control input $u_1(t), u_2(t), u_3(t), u_4(t)$ using controller without barrier function (**red**) and controller with barrier function (**blue**)

control law against a comparable standard sliding mode control law. The numerical results show that the barrier function-based control law achieves a significant reduction in the MSE regulation error while using a similar commanded control magnitude.

TABLE I

PARAMETERS USED IN THE SIMULATION PLANT MODEL

Linear Terms		Quadratic and Cubic Terms	
$b_1 = 557.7$	$L_{11} = -86.1$	$Q_{111} = 1.8$	$Q_{414} = 2.9$
$b_2 = 1016.9$	$L_{22} = -392.4$	$Q_{121} = -2.2$	$Q_{424} = -9.8$
$b_3 = 41.0$	$L_{23} = 263.9$	$Q_{131} = -2.3$	$Q_{434} = 6.3$
$b_4 = -628.9$	$L_{32} = -218.3$	$Q_{141} = -6.8$	$Q_{444} = -7.3$
	$L_{33} = -7.6$	$Q_{212} = 75.0$	
	$L_{41} = 43.4$	$Q_{313} = 5.0$	$R_2 = -2.5$
	$L_{44} = -113.5$	$Q_{314} = 3.9$	$R_3 = -0.2$

ACKNOWLEDGMENT

This research is supported in part by NSF award number 1809790.

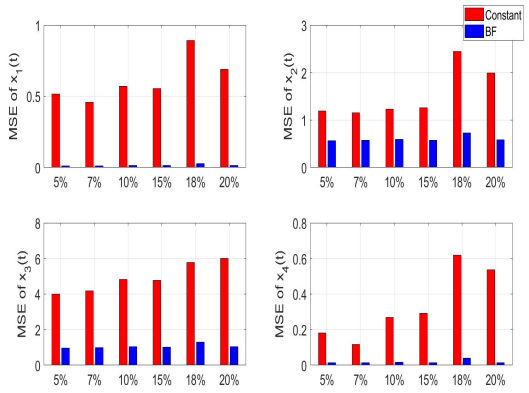

Fig. 3. Average mean squared error (MSE) during closed-loop operation over 10 iterations of randomized time varying parameter uncertainty using the proposed barrier function-based controller (blue) and a standard sliding mode controller (red).

REFERENCES

[1] S. Scharnowski, M. Bosyk, F. F. Schrijer, and B. W. van Oudheusden, "Passive flow control for the load reduction of transonic launcher afterbodies," AIAA Journal, vol. 57, no. 5, pp. 1818–1825, 2019.

[2] S. Acarer, "Peak lift-to-drag ratio enhancement of the du12w262 airfoil by passive flow control and its impact on horizontal and vertical axis wind turbines," Energy, p. 117659, 2020.

[3] J. Song, Z. Zuo, and M. Basin, "New class kfunction-based adaptive sliding mode control design," arXiv preprint arXiv:2012.02633, 2020.

[4] M. Khan and A. Chatterjee, "Gaussian control barrier functions: Safe learning and control," in 2020 59th IEEE Conference on Decision and Control (CDC), pp. 3316–3322, IEEE, 2020.

[5] M. F. Reis, A. P. Aguiar, and P. Tabuada, "Control barrier function-based quadratic programs introduce undesirable asymptotically stable equilibria," IEEE Control Systems Letters, vol. 5, no. 2, pp. 731–736, 2020.

[6] K. B. Kidambi, N. Ramos-Pedroza, W. MacKunis, and S. V. Drakunov, "Robust nonlinear estimation and control of fluid flow velocity fields," in 2016 IEEE 55th Conference on Decision and Control (CDC), pp. 6727–6732, IEEE, 2016.

[7] K. B. Kidambi, N. Ramos-Pedroza, W. MacKunis, and S. V. Drakunov, "A closed-loop nonlinear control and sliding mode estimation strategy for fluid flow regulation," International Journal of Robust and Nonlinear Control, vol. 29, no. 3, pp. 779–792, 2019.

[8] A. Kossery Jayaprakash, W. MacKunis, V. Golubev, and O. Stalnov, "Reduced-order dynamic modeling and robust nonlinear control of fluid flow velocity fields," in 2021 60th IEEE Conference on Decision and Control (CDC), pp. 3978–3983, 2021.

[9] C. K. Batchelor and G. Batchelor, An introduction to fluid dynamics. Cambridge university press, 2000.

[10] C. Kasnakoğlu, A. Serrani, and M. Ö. Efe, "Control input separation by actuation mode expansion for flow control problems," International Journal of Control, vol. 81, no. 9, pp. 1475–1492, 2008.

[11] C. Kasnakoğlu, R. C. Camphouse, and A. Serrani, "Reduced-order model-based feedback control of flow over an obstacle using center manifold methods," Journal of dynamic systems, measurement, and control, vol. 131, no. 1, 2009.

[12] K. B. Kidambi, W. MacKunis, S. V. Drakunov, and V. Golubev, "Sliding mode estimation and closed-loop active flow control under actuator uncertainty," International Journal of Robust and Nonlinear Control, vol. 30, no. 16, pp. 6645–6660, 2020.

[13] H. Obeid, L. Fridman, S. Laghrouche, and M. Harmouche, "Barrier function-based adaptive integral sliding mode control," in 2018 IEEE Conference on Decision and Control (CDC), pp. 5946–5950, IEEE, 2018.

[14] S. V. Gordeyev and F. O. Thomas, "A temporal proper decomposition (tpod) for closed-loop flow control," Experiments in fluids, vol. 54, no. 3, pp. 1–16, 2013.